

# Heralded ultrafast generation of macroscopic quantum states in matter with bright squeezed vacuum light

Shohei Imai

Department of Physics, University of Tokyo, Hongo, Tokyo 113-0033, Japan  
 shohei.imai@phys.s.u-tokyo.ac.jp

May 29, 2026

## Abstract

We show that bright squeezed vacuum light, combined with a single-shot quadrature measurement of the post-interaction light, enables the ultrafast generation of macroscopic quantum states in matter. Although in the weak-coupling regime multiphoton quantum light leaves the unconditional matter state as a classical mixture due to light–matter entanglement, quadrature-based heralding prepares the matter in a Gaussian-weighted quantum superposition. For an ensemble of resonantly electric-dipole-coupled two-level systems, this heralding dynamics acts as a Gaussian filter with respect to the electric polarization, with brighter squeezed-vacuum light accelerating the preparation of the zero-eigenvalue Dicke state. Counter-rotating terms further drive a stroboscopic transition from this Dicke state to a cat-like state. Our results open a route to ultrafast engineering of macroscopic quantum matter with strong-field quantum light.

## 1 Introduction

Macroscopic quantumness lies at the heart of fundamental physics, serving as a bridge between the classical (macroscopic) and quantum (microscopic) worlds and opening new frontiers for future research [1–4]. Moreover, its ability to surpass classical limits facilitates practical applications in quantum computing [5, 6] and quantum metrology [7–10]. However, such macroscopic nonclassicality is intrinsically fragile against interactions with the environment [11, 12]. This motivates an approach in which macroscopic quantum states are generated on timescales shorter than those of relaxation and dephasing.

Recent advances in strong-field quantum light make this approach increasingly feasible. Ultrafast quantum optics is developing rapidly [13–18], driven by the realization of Schrödinger cat or kitten states of light through the combination of high-harmonic generation and quantum measurement [19–23], and of bright squeezed vacuum (BSV) light containing as many as  $10^{13}$  photons per mode [24–26]. Correspondingly, studies exploring the interaction between matter and strong-field quantum light have become increasingly active, including the enhancement of nonlinear effects arising from the super-Poissonian photon statistics of BSV [27], high-harmonic generation driven by BSV [28–34], BSV-driven electron dynamics [35, 36] and photoemission [37, 38], as well as second-harmonic generation [39] and electron dynamics [40, 41] driven by cat-state light.

However, quantum light gives rise to strong light–matter entanglement. Consequently, discarding the information carried by the light after the interaction reduces the matter subsystem to a classically mixed state. To harness the latent quantum character of the matter system, one therefore needs heralding that exploits the information encoded in its entanglement with light. Indeed, Ref. [41] showed that, by performing single-shot projective measurements of photon-number parity or quadrature on the post-interaction light, one can induce a Rabi-oscillation cat state under driving by a macroscopic Schrödinger cat state of light.

In this paper, we show that single-shot quadrature measurements of the post-interaction BSV light herald the ultrafast preparation of macroscopic quantum states of matter that are inaccessible in the corresponding unconditional dynamics. We develop a general theory for BSV-driven dynamics by combining the external-field approximation (XFA), which is valid for multiphoton light as well as the realistic weak electron–photon coupling [40, 41], with the Janszky representation of the squeezed-vacuum (SV) state [42] (Sec. 3). Based on this effective theory, we derive that the quadrature-heralded state of matter is a Gaussian-weighted quantum superposition of matter states driven by classical light [Eq. (18)].

Applying this XFA theory to the Tavis–Cummings (TC) model, the most basic electric-dipole-coupled system [43], we find that quadrature-heralded matter dynamics is described as an ultrafast Gaussian filter [Eq. (24)] with respect to the collective electric polarization (or polarization current). The resulting state is a Dicke state with zero eigenvalue of that macroscopic observable. Furthermore, when finite measurement resolution is taken into account, the success-probability-weighted quantum Fisher information (QFI) scales as  $N^{3/2}$  with the particle number  $N$ , implying metrological performance beyond the standard quantum limit (SQL) (Sec. 4.3). We also analyze the Dicke model [44, 45] beyond the rotating-wave approximation (RWA) and show that the counter-rotating terms drive a stroboscopic transition from the Dicke state to a  $z$ -spin-polarized cat-like state (Sec. 5). Overall, this work offers a matter-response perspective on a fundamental question in strong-field quantum optics: what is genuinely quantum in the phenomena induced by BSV light?

Unlike previous schemes for quantum state generation using SV light or optical measurements, our framework combines a macroscopic matter system with ultrafast generation enabled by strong fields, a basic electric-dipole coupling, and a single-shot optical readout. Previous studies using SV light have reported spin squeezing in small systems [46], conditional state generation by continuous quantum nondemolition (QND) optical measurement [47], squeezing transfer by complete light absorption [48, 49], long-time steady states under incoherent noise (a broadband bath) [50], and quantum-filtering formulations [51]. Other than SV light, proposed schemes have also considered QND-based protocols [52–64], light–matter disentanglement with quantum erasure [65], and spin-1 ensembles [66].

The remainder of this paper is organized as follows. Section 2 reviews the preliminaries, including the formulation of the XFA for general quantum light (Sec. 2.1) and the Janszky representation, which expresses the SV state as a compact superposition of coherent states (Sec. 2.2). Section 3 formulates the XFA theory for BSV-driven dynamics and derives general expressions for unconditional states (Sec. 3.1) and heralded states (Sec. 3.2). Section 4 applies this theory to the TC model and analyzes optically heralded ultrafast matter dynamics. It also discusses the measurement resolution and success probability (Sec. 4.3) and assesses the validity of the XFA by comparison with exact numerical calculations (Sec. 4.4). Section 5 extends the analysis to the Dicke model and examines the effects of the counter-rotating terms. Section 6 presents the conclusions.

## 2 Preliminaries

### 2.1 External-field approximation (XFA)

This section presents a general formulation of the XFA, which is valid when the electron–photon coupling is weak. Focusing on ultrafast dynamics induced by strong-field quantum light, we analyze the time evolution of the pure state of the total light–matter coupling system while neglecting relaxation and dephasing. The formulation follows Ref. [41]. Within this approach, the weak electron–photon coupling justifies neglecting the backaction from matter on the quantum light, allowing the total state to be expressed as a quantum superposition of matter states driven by classical light.

We first represent the initial state of the quantum light as a superposition of coherent states:

$$|\psi(0)\rangle_p = \int d^2\alpha \chi(\alpha) |\alpha\rangle. \quad (1)$$

Here,  $|\alpha\rangle$  ( $\alpha \in \mathbb{C}$ ) denotes a coherent state satisfying  $\hat{a}|\alpha\rangle = \alpha|\alpha\rangle$ , where  $\hat{a}$  is the bosonic annihilation operator. This property makes coherent states classical states describing laser light. Note that, because the coherent-state basis is overcomplete, the amplitude  $\chi(\alpha)$  is not unique; however, in the zero-coupling limit this nonuniqueness is generally irrelevant for the XFA formulation.

Using this representation, the total-system wave function at time  $t$  can be approximated as

$$|\Psi_{\text{XFA}}(t)\rangle_{\text{mp}} = \frac{1}{\sqrt{\mathcal{N}}} \int d^2\alpha \chi(\alpha) |\psi_{F(\alpha)}(t)\rangle_{\text{m}} |\alpha(t)\rangle_{\text{p}}, \quad (2)$$

where  $\mathcal{N}$  is a normalization constant and  $F(\alpha)$  is the field strength; if the electron–photon coupling constant is  $g$ , then  $F(\alpha) = g\alpha$ . The quantity  $g$  depends on system-specific details such as the optical mode function and the electric-dipole moment. The state  $|\psi_{F(t)}\rangle_{\text{m}}$  denotes the matter state driven by the classical field  $F(\alpha)$ , whose time evolution is determined by the following Schrödinger equation:

$$i\partial_t |\psi_{F(t)}\rangle_{\text{m}} = \hat{H}_{\text{m}}[F(\alpha(t))] |\psi_{F(t)}\rangle_{\text{m}}. \quad (3)$$

Here,  $\hat{H}_{\text{m}}[F(\alpha(t))]$  consists of the bare matter Hamiltonian and the classical-field driving term. When the optical frequency is  $\omega$ , then  $\alpha(t) = \alpha \exp(-i\omega t)$ . The subscripts m, p, and mp denote the Hilbert spaces of matter, photons, and the total system, respectively (omitted when unambiguous).

The XFA becomes asymptotically valid in the thermodynamic limit for the photon field. In this limit, the field strength is kept finite while the coupling constant tends to zero and the photon number tends to infinity:

$$g\sqrt{\langle \hat{n} \rangle} = \text{const}, \quad g \rightarrow 0. \quad (4)$$

As a practical criterion, the XFA works well when the initial photon number  $\langle \hat{n} \rangle$  greatly exceeds the number of excited particles  $N_{\text{exc}}$ , namely,  $\langle \hat{n} \rangle \gg N_{\text{exc}}$ . In addition, because this approximation is based on an iterative expansion of the Born series, the condition  $gt \ll 1$  also provides a useful estimate of its timescale of validity. In summary, the XFA provides a quantum generalization of the external-field picture: it adheres to the superposition principle while neglecting matter-to-light backaction along each classically driven trajectory.

## 2.2 Squeezed vacuum state and its Janszky representation

Here we adopt the Janszky representation [42] as the coherent-state expansion (1) of the SV state. A useful feature of the Janszky representation is that it exploits the overcompleteness of coherent states to simplify an expansion that is, in general, given by a two-dimensional integral over the complex plane into a one-dimensional real integral.

The SV state is defined by

$$|\xi\rangle^{\text{sv}} = e^{\frac{1}{2}(\xi^* \hat{a}^2 - \xi \hat{a}^{\dagger 2})} |0\rangle, \quad (5)$$

where  $\xi = r \exp(i\vartheta)$  is the squeezing parameter. Below, we set the angle  $\vartheta = 0$  and consider real  $r$  only.

The Janszky representation of the SV state is given by [42]

$$|r\rangle^{\text{sv}} = \int_{-\infty}^{\infty} \frac{dp}{\sqrt{2\pi \sinh r}} e^{-\frac{\coth r - 1}{2} p^2} |ip\rangle. \quad (6)$$

This expression shows that the SV state can be written as a Gaussian-weighted quantum superposition of coherent states, with a width determined by the squeezing parameter  $r$ .

### 3 General theory for BSV-induced matter dynamics

Based on the formulation above, we derive the XFA effective theory for BSV-light driving. The key control parameter in this theory is the effective field strength of the SV light,

$$F_c \equiv g e^r. \quad (7)$$

The corresponding photonic thermodynamic limit (4) becomes

$$F_c = \text{const}, \quad g \rightarrow 0. \quad (8)$$

In this limit, the SV Janszky representation can be rewritten, with  $F = gp$ , as

$$|r\rangle^{\text{sv}} \stackrel{g \rightarrow 0}{=} \int_{-\infty}^{\infty} \frac{dF}{\sqrt{\pi g F_c}} e^{-(F/F_c)^2} |iF/g\rangle. \quad (9)$$

That is, the SV state is represented as a superposition of coherent states weighted by a Gaussian distribution with width  $F_c$ . At the same time, the total-system wave function becomes

$$|\Psi_{\text{XFA}}(t)\rangle_{\text{mp}} = \int_{-\infty}^{\infty} \frac{dF}{\sqrt{\pi g F_c}} e^{-(F/F_c)^2} |\psi_{iF}(t)\rangle_{\text{m}} |iF(t)/g\rangle_{\text{p}}. \quad (10)$$

This equation indicates that light–matter entanglement is formed through the quantum superposition of light and matter states labeled by the field strength  $F$ .

#### 3.1 Unconditional dynamics

We first consider unconditional matter dynamics without any measurement on the light. The matter state is described by the reduced density matrix obtained by tracing out the photonic degrees of freedom:

$$\hat{\rho}_{\text{m}}(t) = \text{Tr}_{\text{p}} [|\Psi(t)\rangle_{\text{mp}} \langle \Psi(t)|]. \quad (11)$$

By using the orthogonality of coherent states in the photonic thermodynamic limit (4),  $\langle iF/g | iF'/g \rangle \stackrel{g \rightarrow 0}{=} \sqrt{2\pi} g \delta(F - F')$ , the unconditional matter density matrix follows from Eq. (10) as

$$\hat{\rho}_{\text{m}} = \int \frac{dF}{\sqrt{\pi/2} F_c} e^{-2(F/F_c)^2} |\psi_{iF}\rangle \langle \psi_{iF}|. \quad (12)$$

Thus, the matter density matrix is a Gaussian-weighted classical mixture over the  $F$ -diagonal states  $|\psi_{iF}\rangle \langle \psi_{iF}|$ . If no intrinsic interparticle interaction is present, classical-light driving does not increase the matter-side quantumness (such as entanglement) contained in each  $|\psi_{iF}\rangle$ . In addition, convex quantum measures do not increase under classical mixtures with positive weights. It therefore follows that no nonclassical phenomenon emerges in unconditional matter dynamics driven solely by SV light. This conclusion is consistent with Refs. [40, 41], which studied electronically driven systems under Schrödinger cat-state light, and with Ref. [67], which discussed the limitations of approximations based on the Husimi function.

#### 3.2 Heralded dynamics

Next, we perform a measurement on the light and derive the matter state conditioned on the outcome. The measurement is described by Kraus operators  $\hat{M}_{\mu}$  labeled by outcome  $\mu$ , and the corresponding effects

$\hat{E}_\mu = \hat{M}_\mu^\dagger \hat{M}_\mu$  satisfy  $\sum_\mu \hat{E}_\mu = \mathbb{1}$  [68, 69]. Using these operators, the heralded matter density matrix at time  $t$  is given by

$$\hat{\rho}_m^\mu(t) = \frac{\text{Tr}_p \left[ \hat{M}_\mu |\Psi(t)\rangle_{\text{mp}} {}_{\text{mp}}\langle \Psi(t) | \hat{M}_\mu^\dagger \right]}{{}_{\text{mp}}\langle \Psi(t) | \hat{E}_\mu | \Psi(t)\rangle_{\text{mp}}}. \quad (13)$$

Performing a suitable measurement on the light can disentangle the light–matter system while preserving the matter’s quantum superposition. Here we consider measurements of an optical quadrature. The quadrature operator with axis angle  $\varphi$  is defined as

$$\hat{q}_\varphi = [e^{-i\varphi} \hat{a} + e^{i\varphi} \hat{a}^\dagger] / \sqrt{2}. \quad (14)$$

Let  $|q; \varphi\rangle$  denote the eigenstate with eigenvalue  $q \in \mathbb{R}$ . Its overlap with a coherent state  $|\alpha\rangle$  is  $\langle q; \varphi | \alpha \rangle = \pi^{-1/4} e^{-iq_0 p_0 + i\sqrt{2}p_0 q} e^{-(q - \sqrt{2}q_0)^2/2}$ , where  $\alpha \exp(-i\varphi) = q_0 + ip_0$ .

An ideal projective measurement of the quadrature is represented by the Kraus operator

$$\hat{M}_q^\varphi = |0\rangle\langle q; \varphi|. \quad (15)$$

Choosing the quadrature angle in the rotating frame of the harmonic oscillator ( $\varphi = -\omega t$ ) and introducing the scale-invariant outcome  $\tilde{q} = q/g$ , Eq. (10) shows that the heralded matter state can be described using the following unnormalized vector:

$$|\psi^q(t)\rangle_m \equiv {}_p\langle q; \varphi | \Psi(t)\rangle_{\text{mp}}. \quad (16)$$

The success probability density for realizing this  $q$ -heralded state is then

$$P(q) = \langle \psi^q | \psi^q \rangle. \quad (17)$$

Let  $|\psi_{iF}(t)\rangle_m = \hat{U}_F(t) |\psi(0)\rangle_m$  denote the time evolution of the classically driven state with field strength  $F$ . We then define the  $q$ -heralded time-evolution operator as follows:

$$|\psi^q(t)\rangle_m \equiv \hat{\mathcal{U}}^q(t) |\psi(0)\rangle_m, \quad \hat{\mathcal{U}}^q(t) \stackrel{\tilde{q}=\text{const.}}{=} \int \frac{dF}{\pi^{3/4} \sqrt{gF_c}} e^{-(F/F_c)^2} e^{iF\sqrt{2}\tilde{q}} \hat{U}_F(t). \quad (18)$$

Unlike the unconditional case (12), this effective time-evolution operator shows that the  $q$ -heralded state  $|\psi^q(t)\rangle_m$  is a Gaussian-weighted quantum superposition of classically driven states  $|\psi_{iF}(t)\rangle_m$ . The nature of the resulting matter state depends on the details of the classically driven evolution  $\hat{U}_F(t)$ . In Sec. 4 we show that this yields a Dicke state in the TC model, while Sec. 5 demonstrates a stroboscopic cat-like state in the Dicke model.

## 4 Application to the Tavis–Cummings model

In this section we analyze the TC model to study concrete matter dynamics. The model describes the interaction between a resonant single-mode photon field and an ensemble of  $N$  independent particles treated as electric-dipole-coupled two-level electronic states (including atoms, excitons, and electron–hole pairs) within the RWA. After introducing the model and the observables used in the analysis in Sec. 4.1, we study quadrature-heralded matter dynamics in Sec. 4.2, measurement resolution and success probability in Sec. 4.3, and the validity of the XFA in Sec. 4.4. Unless stated otherwise, the dynamics below is analyzed in the rotating frame at frequency  $\omega$ .

## 4.1 Model and observables

We define the  $N$ -particle TC model [43] as

$$\hat{H}_{\text{TC}} = \omega \hat{a}^\dagger \hat{a} + \sum_{j=1}^N \Delta \hat{S}_j^z - ig \sum_j \left( \hat{a} \hat{S}_j^+ - \hat{a}^\dagger \hat{S}_j^- \right). \quad (19)$$

Here,  $\hat{S}_j^b = \sigma_j^b / 2$  ( $b = x, y, z$ ) is the spin-1/2 operator representing the  $j$ th electric-dipole-coupled two-level state, and  $\sigma^b$  is a Pauli matrix ( $\hat{S}_j^\pm = \hat{S}_j^x \pm i\hat{S}_j^y$ ). The parameter  $\Delta$  is the level spacing, and  $g$  is the electron–photon coupling constant. The first and second terms are the free Hamiltonians of the photon field and matter system, respectively, and the third term is the RWA interaction between the electric field and the polarization. We consider the resonance condition  $\omega = \Delta$ , use  $\omega$  as the energy unit, and write  $\omega = 1$  unless otherwise noted. We also restrict attention to even  $N$ .

The classically driven matter state  $|\psi_{iF}(t)\rangle_m$  evolves according to

$$\hat{H}_{\text{TC},m}[iF] = \sum_j \Delta \hat{S}_j^z + \sum_j \left( F(t) \hat{S}_j^+ + F(t)^* \hat{S}_j^- \right), \quad (20)$$

which is obtained by replacing  $\hat{a} \rightarrow i(F/g)$  in Eq. (19). Here,  $F(t) = F \exp(-i\omega t)$ . In the  $\omega$ -rotating frame, the corresponding time-evolution operator is

$$\hat{U}_{\text{TC},F}(t) = e^{-i2F\hat{J}^x t}, \quad (21)$$

where  $\hat{J} = \sum_i \hat{S}_i$  is the collective spin operator.

We take the initial state to be the direct product of the matter ground state, the all-spin-down state  $|\downarrow\downarrow \cdots \downarrow\rangle$ , and the SV state of light  $|r\rangle^{\text{sv}}$ . Since the TC model conserves the total spin, it is convenient to use the Dicke basis. For total spin  $J = N/2$ , the  $b$ -axis Dicke states  $\{|J, m\rangle^b \mid m = -J, \dots, J\}$  satisfy  $\hat{J}^2 |J, m\rangle^b = J(J+1) |J, m\rangle^b$  and  $\hat{J}^b |J, m\rangle^b = m |J, m\rangle^b$  for  $b = x, y, z$ .

Although many measures of quantumness in many-body quantum systems are proposed [3], we employ the quantum Fisher information (QFI) [9, 70, 71], which is well suited for quantifying the number of entangled particles, and the spin Wigner function [72, 73], which is convenient for visualizing quantum states. The QFI is defined as

$$\mathcal{F}_Q = \max_{\hat{A}} \sum_{i,j} 2 \frac{(\lambda_i - \lambda_j)^2}{\lambda_i + \lambda_j} |\langle \lambda_i | \hat{A} | \lambda_j \rangle|^2. \quad (22)$$

Here,  $\hat{A}$  is an arbitrary additive observable, and  $\lambda_i$  and  $|\lambda_i\rangle$  are the  $i$ th eigenvalue and eigenvector of a density matrix  $\hat{\rho}$ . For a pure state,  $\mathcal{F}_Q = \max_{\hat{A}} [4(\langle \hat{A}^2 \rangle - \langle \hat{A} \rangle^2)]$  holds. An important feature of the QFI is that if the QFI density  $\mathcal{F}_Q/N$  exceeds a positive integer  $k$ , then one can infer that at least  $k+1$  particles are entangled [74–77]. Thus macroscopic quantumness is present when the QFI density is extensive, namely,  $\mathcal{F}_Q/N \propto N$ .

Following Ref. [78], we define the spin Wigner function as

$$W(\theta, \phi) = \text{Tr}[\hat{\rho} \hat{\Delta}(\theta, \phi)], \quad \hat{\Delta}(\theta, \phi) = \sum_{m=-J}^J \left( \sum_{j=0}^{2J} \frac{2j+1}{2J+1} C_{Jm;j0}^{Jm} \right) \hat{R}(\theta, \phi) |J, m\rangle^z \langle J, m| \hat{R}^\dagger(\theta, \phi), \quad (23)$$

where  $\hat{R}(\theta, \phi)$  is the rotation operator about the axis  $\mathbf{l} = (-\sin \phi, \cos \phi, 0)$ , given by  $\hat{R}(\theta, \phi) = e^{i\phi \hat{J}^z} e^{i\theta \hat{J}^y} = e^{-i\theta \mathbf{l} \cdot \hat{J}}$ , and  $C_{j_1, m_1; j_2, m_2}^{J, M}$  denotes a Clebsch–Gordan coefficient.

## 4.2 Quadrature-heralded dynamics

We derive the heralded time-evolution operator  $\hat{\mathcal{U}}_{\text{TC}}^q(t)$  for the matter system conditioned on a quadrature outcome  $q$ . From the classically driven time-evolution operator  $\hat{U}_{\text{TC},F}(t)$  [Eq. (21)] and Eq. (18), we obtain

$$\hat{\mathcal{U}}_{\text{TC}}^q(t) = \sqrt{\frac{F_c}{\sqrt{\pi}g}} e^{-(F_c t)^2 [\hat{J}^x - \tilde{q}/(\sqrt{2}t)]^2}. \quad (24)$$

This shows that SV-light driving followed by a single-shot quadrature projective measurement of the light yields an effective Gaussian filter with respect to  $\hat{J}^x$ , or equivalently, imaginary-time one-axis twisting [79], for the matter system. For  $\tilde{q} = 0$ , this filter selects the  $\hat{J}^x = 0$  eigenspace of the collective electric-polarization operator, thereby driving the state toward the  $x$ -axis Dicke state  $|J, 0\rangle^x$ . Returning to the laboratory frame, this corresponds to the zero-eigenvalue state of  $\cos(\omega t)\hat{J}^x + \sin(\omega t)\hat{J}^y$ , where  $\hat{J}^y$  is the polarization-current operator. Moreover, because the asymptotic rate increases with the effective field strength  $F_c$  [Eq. (7)], BSV light enables ultrafast Dicke-state preparation. This distinguishes the present mechanism from Gaussian filters based on conventional QND measurements [55, 60, 61, 64] and from imaginary-time one-axis twisting in open systems [80, 81]. Even for outcomes  $\tilde{q} \neq 0$ , the dynamics likewise converges to the  $\hat{J}^x = 0$  eigenstate in the long-time regime  $t \gg |\tilde{q}|$ .

We now analyze the QFI dynamics starting from the initial matter state  $|J, -J\rangle^z$ . In the rotating frame, the additive observable that maximizes the QFI (22) is  $\hat{A} = \hat{J}^y$ . By expanding the quadrature-heralded state vector  $|\psi^q(t)\rangle$  [Eq. (18)] in the  $x$ -axis Dicke basis, we obtain

$$\mathcal{F}_Q = N + 2(1 - e^{-2\tau^2}) \frac{\sum_{m=-J}^J (J^2 - m^2) |c_m|^2}{\sum_{m=-J}^J |c_m|^2}, \quad (25)$$

where  $|\psi^q(t)\rangle = \sum_m c_m |J, m\rangle^x$  with  $c_m = 2^{-J} \sqrt{\binom{2J}{J+m}} \exp[-\tau^2(m - \mu)^2]$ ,  $\tau = F_c t$ , and  $\mu = \tilde{q}/(\sqrt{2}t)$ . For the outcome  $\tilde{q} = 0$ , this simplifies in the large- $N$  limit to

$$\mathcal{F}_Q \approx N + (1 - e^{-2\tau^2}) \left( \frac{N^2}{2} - \frac{N}{2(1 + N\tau^2)} \right). \quad (26)$$

This expression demonstrates that the QFI density approaches the saturation value  $N/2 + 1$  in a squared-exponential manner, on the timescale of order  $F_c^{-1}$  [Eq. (7)].

Figure 1 shows the numerically calculated quadrature-heralded matter dynamics for  $N = 32$  and  $F_c = g \exp(r) \approx 0.10$  ( $g = 0.005$ ,  $r = 3$ ). Figure 1(a) plots the QFI density  $\mathcal{F}_Q/N$  conditioned on  $\tilde{q} = 0$  [Eq. (25)] as a blue line, together with the corresponding result calculated from the unconditional state  $\hat{\rho}_m$  [Eq. (12)] and Eq. (22) as an orange line. Numerically, the integral over  $F$  is evaluated using the rectangular method. For the unconditional state, the QFI density remains below unity; consequently, the QFI does not reveal any many-body quantumness. By contrast, with quadrature heralding, the QFI density increases rapidly on a timescale  $t \sim F_c^{-1} \approx 10$  and reaches the maximum value  $N/2 + 1$ . This value coincides with the QFI density of the Dicke state  $|J, 0\rangle^x$ . For comparison, the large- $N$  approximation (26) is also shown as a light-blue dashed line, indicating that even at  $N = 32$  it already agrees well with the exact result within the XFA (25).

Figures 1(b)–(d) display spherical color maps of the spin Wigner function  $W(\theta, \phi)$  [Eq. (23)], calculated from the normalized state vector  $|\psi^q\rangle/\sqrt{\langle\psi^q|\psi^q\rangle}$  [Eq. (18)] at the times marked by the arrowheads above Fig. 1(a). In the initial stage of the QFI growth [Fig. 1(b)], the Gaussian distribution, which is localized around  $-z$  at  $t = 0$ , becomes anti-squeezed along the  $y$  axis. Near the end of the QFI growth [Fig. 1(c)], squeezing along the  $x$  axis develops, and negative interference fringes begin to appear around the distribution.

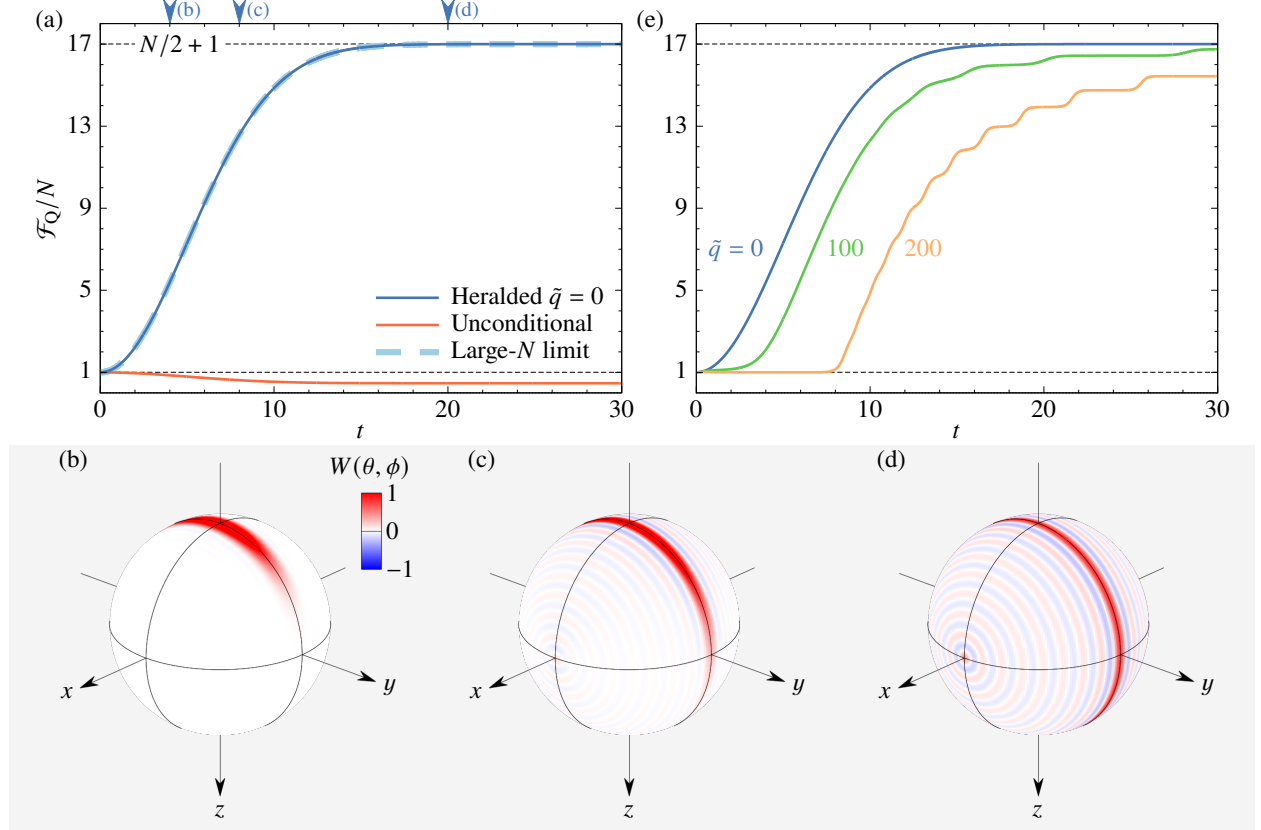


Figure 1: Quadrature-heralded matter dynamics in the TC model (19) within the XFA for  $F_c \approx 0.10$  ( $g = 0.005$ ,  $r = 3$ ) and  $N = 32$ . (a) Time profile of the QFI density  $\mathcal{F}_Q/N$  (blue solid line), for  $\tilde{q} = 0$  [Eq. (25)]. The orange line shows the unconditional case calculated from  $\hat{\rho}_m$  [Eq. (12)]. The light-blue dashed line shows the large- $N$  limit (26). (b)–(d) Spin Wigner function  $W(\theta, \phi)$  [Eq. (23)] at the times indicated in (a). For visualization, only the  $z$  axis is inverted. (e) QFI dynamics for different quadrature outcomes,  $\tilde{q} = q/g = 0, 100, 200$ , corresponding to  $q = 0, 0.5, 1$  for  $g = 0.005$ .

Once the QFI reaches its stationary value [Fig. 1(d)], the distribution becomes rotationally symmetric about the  $x$  axis and is concentrated around the  $yz$  plane, with distinct interference fringes, clearly indicating the formation of the Dicke state  $|J, 0\rangle^x$ . This non-Gaussianity of the Dicke state originates from the finite size of the matter system. Intuitively, the anti-squeezing along the  $y$  axis wraps around the Bloch sphere, inducing self-interference and generating quantumness, thereby producing a rotationally symmetric distribution about the  $x$  axis.

Figure 1(e) shows the dependence of the QFI dynamics on the quadrature measurement outcome. The  $\tilde{q} (= q/g) = 0$  curve (blue) exhibits a squared-exponential increase [see Eq. (26)], whereas the  $\tilde{q} = 100$  (green) and  $\tilde{q} = 200$  (orange) curves show qualitatively similar behavior, except for a delayed onset and step-like increments at later times. The later-time structure visible for  $t \gtrsim 10$  reflects the discrete spectrum of  $\hat{J}^x$ . Importantly, even for outcomes with  $\tilde{q} \neq 0$ , the heralded state eventually converges to the same state  $|J, 0\rangle^x$ , indicating a certain robustness against finite measurement resolution (Sec. 4.3).

### 4.3 Effects of measurement resolution and success probability

In this section we investigate the effects of measurement resolution and success probability on the generation of the Dicke state by SV-light driving and quadrature-based heralding. In this paper, a quadrature measurement

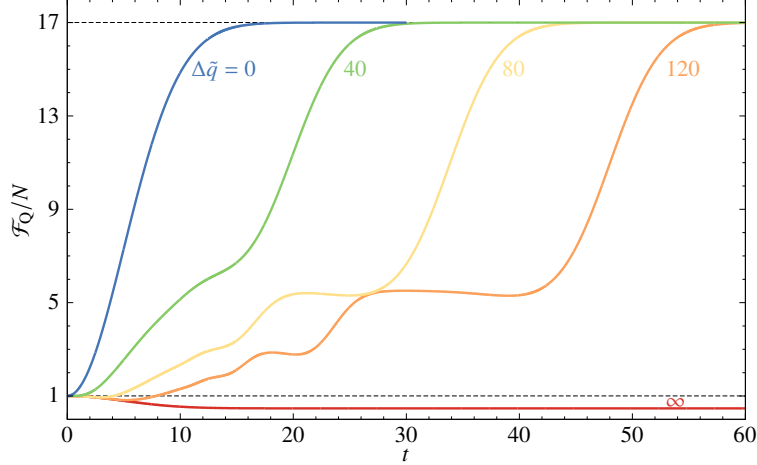


Figure 2: Dependence of the quadrature-heralded QFI density  $\mathcal{F}_Q/N$  on the measurement resolution  $\Delta\tilde{q}$  in the TC model (19) within the XFA for  $F_c \approx 0.10$  ( $g = 0.005$ ,  $r = 3$ ),  $\tilde{q} = 0$ , and  $N = 32$ . The QFI is calculated from  $\hat{\rho}^{q;\Delta q}$  [Eq. (28)]. Given  $g = 0.005$ , the resolutions  $\Delta\tilde{q} = \Delta q/g = 40, 80, 120$  correspond to  $\Delta q = 0.2, 0.4, 0.6$ , respectively.

with resolution  $\Delta q$  is modeled by the following effect:

$$\hat{E}_q^{\varphi;\Delta q} = \int_{q-\Delta q/2}^{q+\Delta q/2} dq' |q'; \varphi\rangle \langle q'; \varphi|. \quad (27)$$

Using this operator and the measurement probability density  $P(q)$  [Eq. (17)], the matter state heralded by an outcome centered at  $q$  with resolution  $\Delta q$  is given by

$$\hat{\rho}^{q;\Delta q} = \frac{\int_{q-\Delta q/2}^{q+\Delta q/2} dq' |\psi^{q'}\rangle \langle \psi^{q'}|}{\int_{q-\Delta q/2}^{q+\Delta q/2} dq' P(q')}. \quad (28)$$

Figure 2 shows the time evolution of the QFI density  $\mathcal{F}_Q/N$  [Eq. (22)] calculated from the matter state  $\hat{\rho}^{q;\Delta q}$  [Eq. (28)] heralded by a finite-resolution quadrature measurement. Since the scaled outcome  $\tilde{q} = q/g$  is the relevant quantity in the XFA (18), the dynamics depends on  $\Delta q$  only through the scaled resolution  $\Delta\tilde{q} = \Delta q/g$ . We set the outcome center to  $\tilde{q} = 0$ . Numerically, the integral over  $q'$  is evaluated using the rectangular method. Overall, the monotonic growth of the ideal measurement  $\Delta\tilde{q} = 0$  is suppressed up to a certain time by finite  $\Delta\tilde{q}$ , but eventually crosses over to the same squared-exponential growth. At early times, larger  $\Delta\tilde{q}$  prolongs the agreement with the unconditional curve (red), corresponding to  $\Delta\tilde{q} \rightarrow \infty$ . This is followed by stepwise increases arising from the discreteness of  $\hat{J}^x$ , as in the case of nonzero outcomes  $\tilde{q} \neq 0$ . Finally, as  $\Delta\tilde{q}$  increases, the waiting time before the onset of squared-exponential growth becomes longer. Below we analyze this behavior separately in the high-resolution limit of small  $\Delta\tilde{q}$  and the coarse-grained limit of large  $\Delta\tilde{q}$ .

### High-resolution limit

We analyze the high-resolution case  $\Delta q \ll 1$  and examine the particle-number  $N$  scaling of the QFI weighted by the success probability. This quantity is important because it directly determines the practically achievable sensitivity in quantum metrology.

For small resolution  $\Delta q \ll 1$ , the probability-weighted QFI can be approximated as

$$\mathcal{F}_Q[\hat{\rho}^{q;\Delta q}] \int_{q-\Delta q/2}^{q+\Delta q/2} dq' P(q') \approx \mathcal{F}_Q \left[ |\psi^q\rangle / \sqrt{\langle \psi^q | \psi^q \rangle} \right] P(q) \Delta q. \quad (29)$$

For the bin centered at  $q = 0$ , the probability density  $P(0) = \langle \psi^0 | \psi^0 \rangle$  reads

$$\langle \psi^0 | \psi^0 \rangle = \frac{F_c}{\sqrt{\pi}g} \sum_m 2^{-N} \binom{2J}{J+m} e^{-2\tau^2 m^2} \approx \begin{cases} \frac{F_c}{\sqrt{\pi}g} \frac{1}{\sqrt{1+N\tau^2}}, & (\tau \ll 1) \\ \frac{F_c}{\sqrt{\pi}g} \frac{1}{\sqrt{\pi N/2}}, & (\tau \gg 1). \end{cases} \quad (30)$$

In either limit, one thus finds  $P(0) \propto N^{-1/2}$ . Meanwhile, Eq. (26) shows that the QFI of the normalized state  $|\psi^q\rangle$  scales as  $\mathcal{F}_Q \propto N^2$  for  $\tau = F_c t \gg 1$ . Accordingly, the probability-weighted QFI scales as

$$\mathcal{F}_Q \left[ |\psi^q\rangle / \sqrt{\langle \psi^q | \psi^q \rangle} \right] P(q) \Delta q \propto N^{3/2}. \quad (31)$$

This result shows that, although the Heisenberg scaling of the Dicke state  $|J, 0\rangle^x$  is weakened by the success probability, the attainable precision still surpasses the SQL.

Although both the SV state and the even cat state consist only of even-photon-number components, they induce matter states with different metrological scalings. For driving with the even cat-state light  $|\alpha_0\rangle + |-\alpha_0\rangle$ , the total-system wave function in the XFA is given by [41]

$$|\Psi_{\text{XFA}}^{\text{cat}}\rangle_{\text{mp}} = \frac{1}{\sqrt{2}} (|\psi_{\alpha_0}\rangle_{\text{m}} |\alpha_0\rangle + |\psi_{-\alpha_0}\rangle_{\text{m}} |-\alpha_0\rangle). \quad (32)$$

The probability density for a quadrature outcome  $q$  is then

$$P^{\text{cat}}(q) = \frac{e^{-q^2}}{2\sqrt{\pi}} \left( 2 + \langle \psi_{\alpha_0} | \psi_{-\alpha_0} \rangle e^{i2\sqrt{2}\alpha_0 q} + \langle \psi_{-\alpha_0} | \psi_{\alpha_0} \rangle e^{-i2\sqrt{2}\alpha_0 q} \right), \quad (33)$$

with  $\alpha_0 \in \mathbb{R}$  and the quadrature angle  $\varphi = -\omega t + \pi/2$ . When the QFI is maximized, namely,  $\langle \psi_{-\alpha_0} | \psi_{\alpha_0} \rangle = 0$ , this reduces to

$$P^{\text{cat}}(q) = \frac{e^{-q^2}}{\sqrt{\pi}}, \quad (34)$$

which is independent of the particle number  $N$ . It follows that

$$\mathcal{F}_Q \left[ (|\psi_{\alpha_0}\rangle + |\psi_{-\alpha_0}\rangle) / \sqrt{2} \right] P^{\text{cat}}(q) \Delta q \propto N^2, \quad (35)$$

so the Heisenberg limit is retained even after including the success probability. Thus, while SV light and even cat-state light consist only of even-photon-number states, even cat-state light can generate stronger nonclassicality in the matter system.

### Coarse-grained limit

Next, we derive the relationship between the measurement resolution  $\Delta q$  and the onset time of the squared-exponential growth of the QFI. At long times, the heralded state can be approximated by a three-component truncation in the  $\hat{J}^x$  basis, involving only  $m = 0, \pm 1$ , because of the Gaussian filtering  $\hat{U}_{\text{TC}}^q(t) \sim \exp[-(F_c t)^2 (\hat{J}^x)^2]$

[Eq. (24)]. Then the  $q$ -heralded state vector follows from Eq. (18) as

$$|\psi^q\rangle \approx \sqrt{\frac{F_c}{\sqrt{\pi}g}} 2^{-J} \left( \sqrt{\binom{2J}{J}} e^{-(F_c \bar{q})^2/2} |J, 0\rangle^x + \sqrt{\binom{2J}{J+1}} e^{-[F_c(\bar{q}-\sqrt{2}t)]^2/2} |J, 1\rangle^x + \sqrt{\binom{2J}{J-1}} e^{-[F_c(\bar{q}+\sqrt{2}t)]^2/2} |J, -1\rangle^x \right). \quad (36)$$

To account for the reduction in the QFI density from  $N/2 + 1$ , it is sufficient to evaluate the diagonal weights of  $|J, \pm 1\rangle^x$ , since these quantify admixtures outside  $|J, 0\rangle^x$ . For either of the diagonal components  $|J, \pm 1\rangle^x \langle J, \pm 1|$  contained in the density matrix  $\hat{\rho}^{q;\Delta q}$  [Eq. (28)], the coefficient is proportional to

$$\int_{-\Delta q/2}^{\Delta q/2} dq' \frac{F_c}{\sqrt{\pi}g} 2^{-N} \binom{2J}{J \pm 1} e^{-F_c^2(q'/g \mp \sqrt{2}t)^2} \approx \frac{1}{2\pi F_c \sqrt{N}} \frac{e^{-2F_c^2[t - \Delta q/(2\sqrt{2}g)]^2}}{t - \Delta q/(2\sqrt{2}g)}, \quad (37)$$

which is an expansion controlled by  $\sqrt{2}F_c[t - \Delta q/(2\sqrt{2}g)] \gg 1$ . Hence, the crossover time is estimated as

$$t \gtrsim \frac{\Delta \bar{q}}{2\sqrt{2}}, \quad (38)$$

beyond which the asymptotic dynamics approaching the Dicke state  $|J, 0\rangle^x$  appear even for finite-resolution measurements.

#### 4.4 Validity of XFA: comparison with total-system simulations

We validate the XFA used above by comparing it with numerical simulations of the total system. We compute the time evolution of the total-system state under the TC Hamiltonian  $\hat{H}_{\text{TC}}$  [Eq. (19)] using a small time step  $\delta t$  as  $|\Psi(t + \delta t)\rangle_{\text{mp}} = \exp(-i\hat{H}\delta t)|\Psi(t)\rangle_{\text{mp}} = \sum_{n=0}^4 (-i\hat{H}\delta t)^n/n! |\Psi(t)\rangle_{\text{mp}} + \mathcal{O}(\delta t^5)$ . The numerical accuracy is controlled by  $\delta t$  and by the truncation maximum photon number  $n_{\text{max}}$  of the photonic Hilbert space. Convergence is confirmed by setting  $(\delta t, n_{\text{max}})$  as:  $(10^{-4}, 2000)$  for  $g = 0.02$  and  $0.015$ ;  $(10^{-4}, 3000)$  for  $g = 0.01$ ; and  $(1.25 \times 10^{-5}, 5000)$  for  $g = 0.005$ .

Figure 3 shows the dependence of the quadrature-heralded QFI density  $\mathcal{F}_Q/N$  dynamics on the electron-photon coupling constant  $g$ , where we assume the ideal projection (15) for  $q = 0$  and the density matrix (13). The squeezing parameter is set to  $r = 3 - \ln(g/0.005)$  so as to keep  $F_c$  [Eq. (7)]. As  $g$  is reduced from 0.02 to 0.005, the full simulation agrees with the XFA (blue dashed curve) over an increasingly long time span. This observation is consistent with the Born-series-based formulation of the XFA, which is justified when  $gt \ll 1$ . The long-time deviation between the exact numerical results and the XFA can be attributed to backaction from the driven matter system onto the quantum light; its physical consequences are summarized in Appendix A.

## 5 Application to the Dicke model

In this section, we analyze the Dicke model [44, 45] as a light-matter coupling model without the RWA. We show that the counter-rotating terms can periodically reshape the heralded Dicke state into a cat-like state.

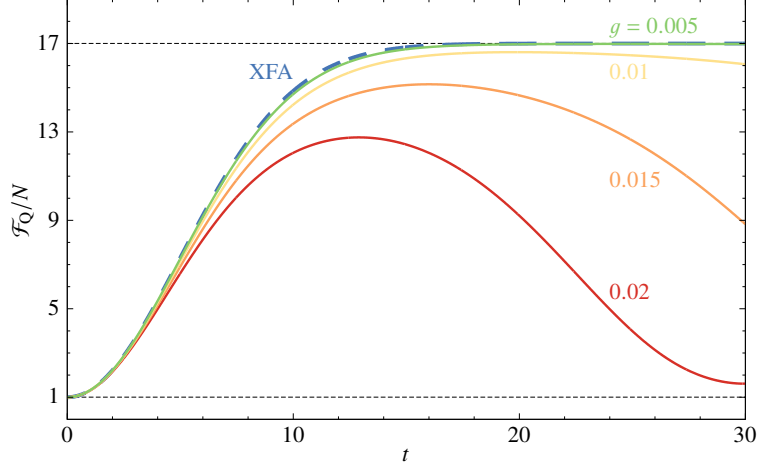


Figure 3: Comparison between the XFA and full light–matter simulations for the quadrature-heralded QFI density  $\mathcal{F}_Q/N$  in the TC model (19). The blue dashed curve shows the XFA result (25), and the solid curves show full numerical simulations for different electron–photon couplings  $g = 0.005, 0.01, 0.015,$  and  $0.02$ . Parameters are set to  $r = 3 - \ln(g/0.005)$ ,  $q = 0$ ,  $\Delta q = 0$ , and  $N = 32$ .

The  $N$ -qubit Dicke model is defined as

$$\hat{H}_D = \omega \hat{a}^\dagger \hat{a} + \sum_{j=1}^N \Delta \hat{S}_j^z - \hat{E} \cdot \hat{P}, \quad (39)$$

$$\hat{E} = iE_0(\hat{a} - \hat{a}^\dagger), \quad \hat{P} = \sum_j d(\hat{S}_j^+ + \hat{S}_j^-). \quad (40)$$

Here,  $\hat{E}$  is the electric-field operator ( $E_0$  is the mode function), and  $\hat{P}$  is the electric-polarization operator ( $d$  is the electric-dipole moment). The TC model (19) is obtained by applying the RWA, which neglects the counter-rotating terms  $\hat{a} \hat{S}_j^-$  and  $\hat{a}^\dagger \hat{S}_j^+$  oscillating at  $2\omega$  in the rotating frame. In this case,  $g = dE_0$ . The RWA is valid when one focuses on the coarse-grained dynamics obtained by averaging over the rapid  $2\omega$  oscillations, or when the field strength  $g\sqrt{\langle \hat{n} \rangle}$  is not too large.

We analyze the quadrature-heralded matter state  $|\psi^q(t)\rangle$  [Eq. (18)] in the Dicke model within the XFA. The matter state  $|\psi_{iF}(t)\rangle$  evolves under the Hamiltonian  $\hat{H}_{D,m}[iF] = \omega \hat{J}^z + 2(Fe^{-i\omega t} + F^*e^{i\omega t})\hat{J}^x$ , obtained by replacing  $\hat{a} \rightarrow i(F/g)$ . Numerically, we diagonalize the single-two-level Hamiltonian  $\hat{h}_{D,m,j}$  ( $\hat{H}_{D,m} = \sum_j \hat{h}_{D,m,j}$ ), evolve each two-level state according to  $|\psi_j(t + \delta t)\rangle = \exp(-i\hat{h}_{D,m,j}\delta t)|\psi_j(t)\rangle$ , and construct the  $N$ -qubit state as their direct product ( $\delta t = 0.01$ ). For the optical quadrature measurement, as in Sec. 4.2, we consider a projective measurement onto a quadrature eigenstate (15).

Figure 4 shows the quadrature-heralded QFI (22) and spin Wigner function (23), calculated from the normalized state vector  $|\psi^q\rangle/\sqrt{\langle \psi^q | \psi^q \rangle}$  [Eq. (18)] for  $\tilde{q} = 0$ . In Fig. 4(a), the QFI exhibits an oscillatory component at frequency  $2\omega$  ( $\omega = 1$ ). For the relatively weak SV field strength,  $F_c = g \exp(r) \approx 0.037$  ( $r = 2$ ,  $g = 0.005$ ), this oscillation remains small, consistent with the RWA results for the TC model [Eq. (26) and Fig. 1(a)]. By contrast, for the stronger field  $F_c \approx 0.27$  ( $r = 4$ ), the oscillation amplitude becomes large, and the QFI density reaches its maximal value  $N$  at certain times. The corresponding spin Wigner functions in Fig. 4(b), taken at the arrow-marked times in Fig. 4(a), display Gaussian lobes localized at the  $\pm z$  axes together with clear interference fringes on the  $xy$  plane. These indicate the formation of a  $z$ -polarized cat-like state, namely a Greenberger–Horne–Zeilinger (GHZ)-like state [82].

To understand heuristically the mechanism of this  $z$ -polarized cat-like state formation, we perform an

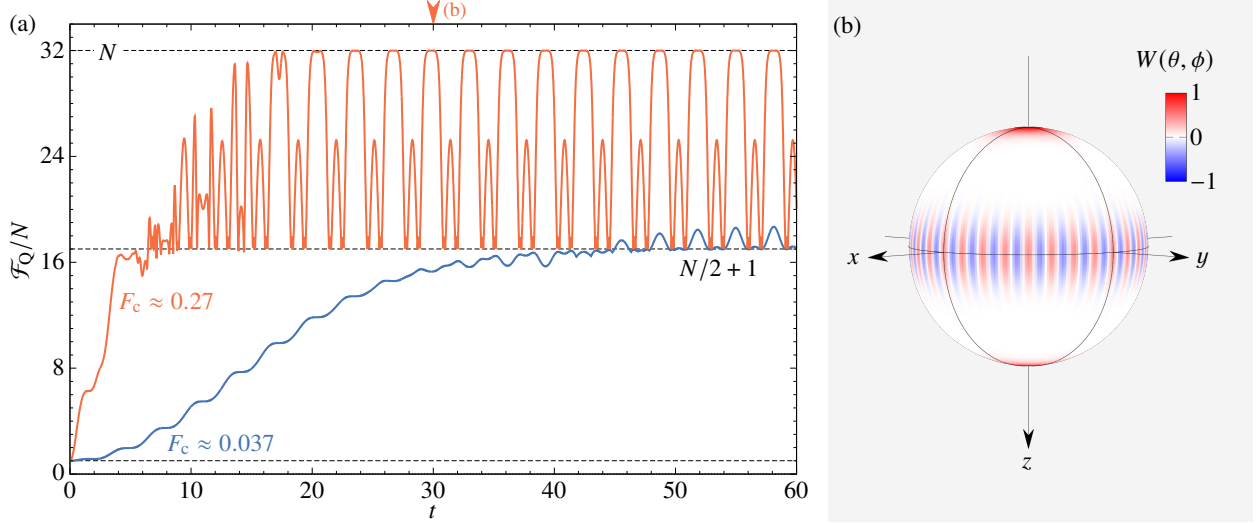


Figure 4: Quadrature-heralded matter dynamics in the Dicke model (39) within the XFA for  $\tilde{q} = 0$  and  $N = 32$ . (a) Time profile of the QFI density  $\mathcal{F}_Q/N$  for  $F_c = g \exp(r) \approx 0.27$  and  $0.037$ , corresponding to  $r = 4$  and  $2$  for  $g = 0.005$ . (b) Spin Wigner function  $W(\theta, \phi)$  at the time indicated in (a).

analytical calculation using the Floquet–Magnus expansion [83–87]. In this approach, the time-evolution operator  $\hat{U}_{D,F}(t)$  of the Dicke model  $\hat{H}_{D,m}[iF]$  coupled to classical light can be approximated as

$$\hat{U}_{D,F}(t) \approx e^{-i\hat{K}(t)} \hat{U}_{TC,F}(t), \quad (41)$$

$$\hat{K}(t) = \frac{F}{\omega} [\sin(2\omega t)\hat{J}^x + (\cos(2\omega t) - 1)\hat{J}^y]. \quad (42)$$

This approximation decomposes the Dicke-model evolution into the RWA evolution  $\hat{U}_{TC,F}(t)$  [Eq. (21)] and a micromotion operator  $\exp[-i\hat{K}(t)]$  oscillating at frequency  $2\omega$ , and is valid under the condition  $F/\omega \ll 1$ .

We focus on times  $t = (2m+1)\pi/(2\omega)$  ( $m \in \mathbb{N}$ ), at which the noncommutativity between the micromotion operator and the RWA time-evolution operator becomes pronounced. At these times, the  $\tilde{q} = 0$  quadrature-heralded time-evolution operator under the XFA is calculated from Eq. (18) as

$$\hat{\mathcal{U}}_D^{q=0}(t) \propto \sum_{m_y, m_x} e^{-(F_c t)^2 [m_x - m_y/(\omega t)]^2} y \langle J, m_y | J, m_x \rangle^x |J, m_y\rangle^y \langle J, m_x|. \quad (43)$$

Examining the exponential factor, we find that at sufficiently late times ( $t \gg F_c^{-1}$ ) the main contribution first comes from the collective-spin eigenvalue  $m_x = 0$  along the  $x$  axis. This agrees with the RWA result obtained in Sec. 4.2. On top of this, the correction factor from the counter-rotating terms is expressed as

$$\hat{\mathcal{U}}_D^{q=0}(t) \propto e^{-\left(\frac{F_c}{\omega}\right)^2 (\hat{J}^y)^2} |J, 0\rangle^x \langle J, 0|. \quad (44)$$

The dynamics can therefore be interpreted as a two-step filtering process: Gaussian filtering first selects  $|J, 0\rangle^x$  in the  $x$ -spin basis, and the counter-rotating terms then impose an additional Gaussian filter on the  $y$  spin with strength  $F_c/\omega$ . When the SV field strength  $F_c/\omega$  is small, this additional filtering along the  $y$  axis has only a minor effect, as seen in the blue curve in Fig. 4(a). As  $F_c/\omega$  increases, however, the spin Wigner distribution, initially spread isotropically over the  $yz$  plane, is filtered toward the eigenspace of  $\hat{J}^y = 0$ , whose weight is concentrated around the  $xz$  plane. As a result, the weight shifts toward the  $\pm z$  directions, and a

$z$ -polarized cat-like state emerges during this intermediate process.

This mechanism admits a simple analytical interpretation, particularly for  $F_c/\omega = N^{-1/2}$ . Expanding  $|J, 0\rangle^x = \sum_m c_m |J, m\rangle^y$ , one finds that within the Gaussian filtering  $\exp(-m^2/N)$  the coefficients  $c_m$  can be regarded as nearly uniform magnitude, up to symmetry-related phases. That is,  $c_m \propto N^{-1/2} \Pi_J(m)$ , where  $\Pi_J(m) = [1 + (-1)^{J-m}]/2$ . Combining this with the large- $N$  expression  $|J, \pm J\rangle^z \propto N^{-1/4} \sum_m (\pm 1)^m \exp(-m^2/N) |J, m\rangle^y$ , we obtain

$$e^{-(\hat{J}^y)^2/N} |J, 0\rangle^x \propto N^{-1/4} \left( |J, J\rangle^z + (-1)^J |J, -J\rangle^z \right). \quad (45)$$

The above argument clarifies that the counter-rotating terms in the Dicke model drive a stroboscopic transformation of the  $x$ -axis Dicke state  $|J, 0\rangle^x$  into the  $z$ -polarized cat-like state.

## 6 Conclusion

We propose a framework for the ultrafast generation of macroscopic quantum states in matter using bright squeezed vacuum (BSV) light. In the weak-coupling, multiphoton regime (the photonic thermodynamic limit), we show that driving with BSV light alone yields only a classical mixture of classically driven states because of light–matter entanglement. We then demonstrate that, when the system is heralded by the outcome of a single-shot quadrature projective measurement on the post-interaction squeezed-vacuum (SV) light, the resulting matter state generally becomes a Gaussian-weighted quantum superposition. For a minimal model with electric-field–polarization coupling, the heralded matter system is filtered into the zero-eigenspace of the matter observable coupled to light, at a rate proportional to the square root of the photon number in the SV light. The resulting macroscopic quantum states also exhibit metrological performance beyond the standard quantum limit. These results suggest that macroscopic quantum states can be prepared on ultrashort timescales, before relaxation or dephasing becomes dominant, thereby opening a new route to ultrafast quantum metrology.

The proposed mechanism for generating macroscopic quantum states in matter can be extended to a broader class of matter systems, including atoms, molecules, and solid-state electronic systems. In general, the increasingly complex dependence of the classically driven time-evolution operator  $\hat{U}_F(t)$  on the field strength  $F$  leads to a richer variety of matter states, as illustrated by the nonlinear effects of the counter-rotating terms in Sec. 5. Conversely, when the exponent of  $\hat{U}_F(t)$  contains only terms linear or quadratic in  $F$ , the quadrature-heralded time-evolution operator  $\hat{U}^q(t)$  [Eq. (18)] can sometimes be evaluated as a Gaussian integral. In such cases, heralding essentially acts as a filter onto the zero-eigenspace of the observable coupled to light. The present framework can therefore also be viewed as a general principle of strong-field quantum-light engineering for designing desired many-body quantum states.

We summarize experimental parameter estimates below. In free-space driving, the electron–photon coupling constant  $g$  depends on the effective mode volume  $V_{\text{eff}}$ . Nevertheless, the standard single-mode expression  $g = d\sqrt{\omega/2\hbar\epsilon_0 V_{\text{eff}}}$  gives a typical scale of  $g/\omega \sim 10^{-8}$ – $10^{-5}$ . In cavity systems,  $g/\omega \sim 10^{-2}$ – $10^{-1}$  is widely available [88]. As for the squeezing parameter  $r$ , directly measured values reach  $r \approx 1.73$  (15 dB) [89]. For recent BSV light, meanwhile, one can infer  $r_{\text{eff}} \approx 15$  from photon numbers  $\langle \hat{n} \rangle \sim 10^{13}$  [24–26], although this is not a direct measurement. Assuming  $\hbar\omega = 1.55$  eV in the optical/infrared range,  $F_c/\omega \gtrsim 0.5$  allows state generation on subfemtosecond, i.e., attosecond, timescales. This can be achieved, for example, either with  $g/\omega \sim 10^{-7}$  and  $\langle \hat{n} \rangle \sim 10^{13}$ , or with  $g/\omega \sim 10^{-1}$  and  $r \sim 1.7$ . Meanwhile, the measurement model in Sec. 4.3 indicates that the required quadrature resolution is  $\Delta q \lesssim 2\sqrt{2}gt$  [Eq. (38)]. To reach the attosecond regime, one likewise needs  $\Delta q \sim \exp(-r)$ . In particular, for BSV light with  $\langle \hat{n} \rangle \sim 10^{13}$ , this requires  $\Delta q \lesssim 10^{-6}$ . Hence, advances in quantum measurement techniques for the multiphoton regime are essential for realizing and observing new attosecond quantum many-body phenomena driven by strong-field quantum

light. Notably, this is also the resolution required to verify the intrinsic quantum nature of the BSV light itself, which is consistent with the idea that resolving the quantum nature of the driving light is a prerequisite for inducing quantum features in the driven system.

As a future direction, it is important to refine the treatment of the mode structure of the light field. In this work, the light interacting with matter is modeled as a single bosonic mode. A more rigorous treatment of scattering, input-output processes, and measurement, however, would require multiple channels corresponding to the input and output ports, as well as continuous spatiotemporal modes in each channel. A natural framework for such an extension is provided by input-output theory [90, 91]. In particular, actual quadrature measurements are implemented through balanced homodyne detection [92–94], and a quantitative assessment of the mode matching with the local oscillator is necessary to evaluate the performance of the ultrafast heralding discussed here. Nevertheless, if a single dominant spatiotemporal mode is effectively selected both in the light–matter interaction and in the measurement of the outgoing light—for example, when a dominant Schmidt mode exists and mode matching with the local oscillator is high—then the single effective-mode description used here should remain a good approximation.

## Acknowledgments

This work was supported by JST FOREST (Grant No. JPMJFR2131) and JSPS KAKENHI (Grant Nos. JP25K17343 and JP26K21749).

## Appendix A Backaction-induced unconditional macroscopic quantum-state generation at late times

We investigate the long-term dynamics of the coupled light–matter system and demonstrate that matter can be driven into a quantum state even without conditioning on optical measurement outcomes, due to the previously neglected backaction of matter on light. Because this action–backaction process is rate-limited by the electron–photon coupling constant  $g$ , it proceeds on a slower timescale than the driving set by the effective field strength  $g\sqrt{\langle\hat{n}\rangle}$  of strong-field quantum light. Accordingly, relaxation and dephasing generally compete with this dynamics; however, in the present analysis, we restrict ourselves to the coherent limit.

Figure 5 shows the dynamics of the unconditional matter density matrix  $\hat{\rho}_m$  [Eq. (11)] calculated from the total-system wave function time-evolved under the TC model (19). The computational method and conditions are the same as those of Fig. 3, with the electron–photon coupling fixed at  $g = 0.005$ . Figure 5(a) shows the time profile of the QFI density  $\mathcal{F}_Q/N$  [Eq. (22)]. In the multiphoton regime  $r = 4$  (dark blue curve), the QFI density does not exceed unity for  $t \lesssim 40$ , consistent with the unconditional XFA results shown as the red curve in Fig. 2. At later times, after once reaching the stationary value  $(N - 1)/[2(N + 1)]$ , the QFI density rises again, which can be interpreted as a manifestation of matter-to-light backaction.

With weaker squeezing and hence fewer photons, backaction influences the dynamics already in the early stage. In the few-photon regime  $r = 0.5$  (light blue curve), the QFI density exhibits a peaked increase. This dynamics can be understood as quantum-state transfer, in which the matter system absorbs all the energy initially contained in the light field, together with its squeezing [48, 49]; see Ref. [41] for the cat-state case.

For  $N = 32$ , the QFI peak originating from this complete energy absorption reaches its maximum around  $r = 1.85$  (blue curve); the peak time scales as  $t_{\text{peak}} \propto 1/g\sqrt{N}$  because of the collective coupling. Figure 5(b) shows the dependence of the time-maximized QFI density,  $\max_t[\mathcal{F}_Q/N]$ , on the squeezing parameter  $r$ . Again, the QFI density is nonmonotonic in  $r$  and exhibits a peak. In particular, the decrease of  $\max_t[\mathcal{F}_Q/N]$  for  $r \gg 1$  is consistent with the XFA conclusion that the quantumness characterized by the QFI does not increase in the unconditional case.

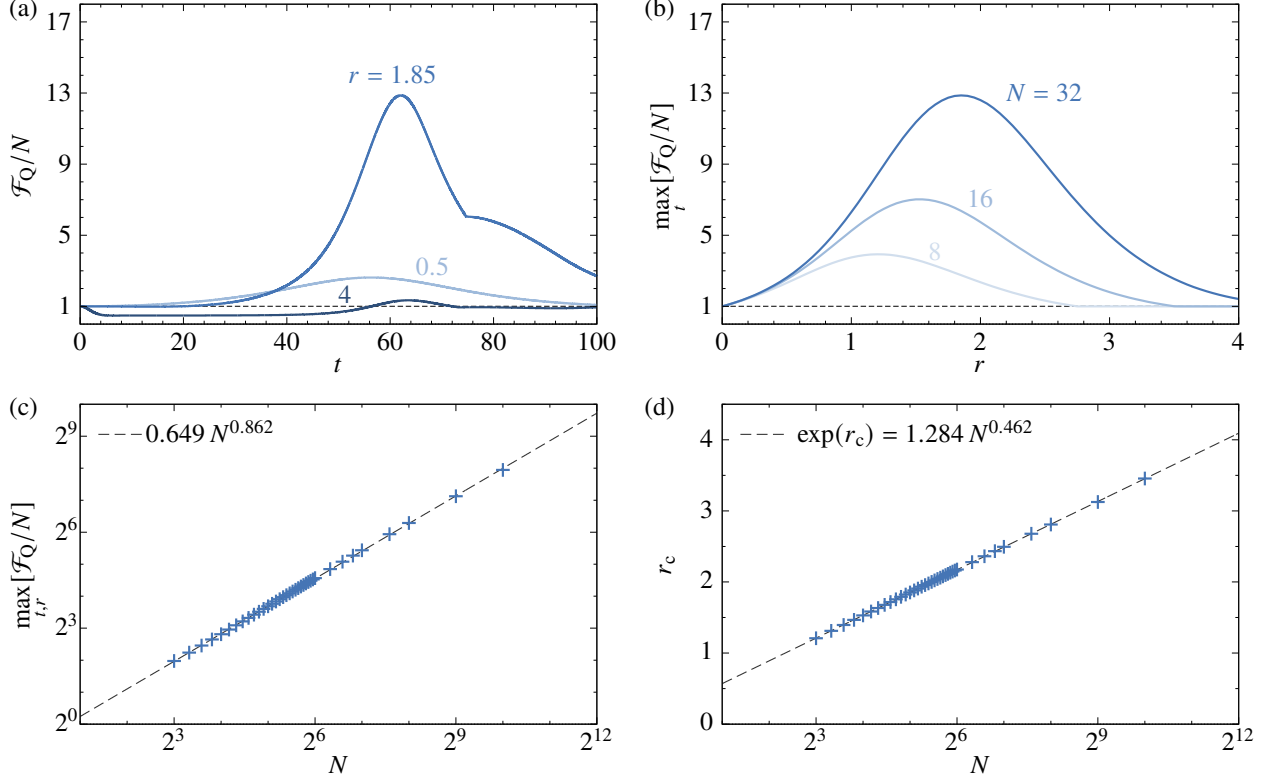


Figure 5: Late-time unconditional matter dynamics in the TC model (19) without the XFA. The electron–photon coupling is fixed at  $g = 0.005$ . (a) Time profile of the QFI density  $\mathcal{F}_Q/N$  calculated from  $\hat{\rho}_m$  [Eq. (11)] for  $N = 32$ . The curves correspond to  $r = 0.5, 1.85$ , and  $4$ . (b) Maximum QFI over time as a function of the squeezing parameter  $r$ . (c) Maximum QFI over time and  $r$  as a function of the particle number  $N$ . (d) Particle-number dependence of the optimal squeezing parameter  $r_c$  that maximizes the QFI.

Figure 5(c) shows the particle-number dependence of this QFI-density peak. The numerical data can be fitted by

$$\max_r \left[ \max_t [\mathcal{F}_Q/N] \right] \approx 0.65 N^{0.86}. \quad (46)$$

Although this does not reach the Heisenberg scaling  $\mathcal{F}_Q \propto N^2$ , it suggests metrological sensitivity beyond the SQL ( $\mathcal{F}_Q \propto N$ ). However, because relaxation and dephasing are neglected here, environmental effects should be carefully considered for this quantum-state formation in the long-time regime ( $t \sim g^{-1}$ ).

Figure 5(d) further shows the particle-number dependence of the optimal squeezing parameter  $r_c$  that maximizes the QFI density. The numerical results are well fitted by

$$r_c \approx 0.46 \ln N + 0.26. \quad (47)$$

## References

- [1] E. Schrödinger, “Die gegenwärtige Situation in der Quantenmechanik”, *Naturwissenschaften* **23**, 807 (1935).
- [2] A. J. Leggett, “Macroscopic Quantum Systems and the Quantum Theory of Measurement”, *Prog. Theor. Phys. Suppl.* **69**, 80 (1980).

- [3] F. Fröwis, P. Sekatski, W. Dür, N. Gisin, and N. Sangouard, “Macroscopic quantum states: Measures, fragility, and implementations”, [Rev. Mod. Phys. \*\*90\*\*, 025004 \(2018\)](#).
- [4] M. Arndt and K. Hornberger, “Testing the limits of quantum mechanical superpositions”, [Nat. Phys. \*\*10\*\*, 271 \(2014\)](#).
- [5] P. Shor, “Algorithms for quantum computation: discrete logarithms and factoring”, in [Proc. 35th Annu. Symp. Found. Comput. Sci.](#) (1994), pp. 124–134.
- [6] L. K. Grover, “A fast quantum mechanical algorithm for database search”, in [Proc. twenty-eighth Annu. ACM Symp. Theory Comput. - STOC '96](#), Vol. Part F1294, March (1996), pp. 212–219.
- [7] C. Helstrom, “Minimum mean-squared error of estimates in quantum statistics”, [Phys. Lett. A \*\*25\*\*, 101 \(1967\)](#).
- [8] C. M. Caves, “Quantum-mechanical noise in an interferometer”, [Phys. Rev. D \*\*23\*\*, 1693 \(1981\)](#).
- [9] S. L. Braunstein and C. M. Caves, “Statistical distance and the geometry of quantum states”, [Phys. Rev. Lett. \*\*72\*\*, 3439 \(1994\)](#).
- [10] V. Giovannetti, S. Lloyd, and L. Maccone, “Quantum-Enhanced Measurements: Beating the Standard Quantum Limit”, [Science \*\*306\*\*, 1330 \(2004\)](#).
- [11] E. Joos and H. D. Zeh, “The emergence of classical properties through interaction with the environment”, [Zeitschrift für Phys. B Condens. Matter \*\*59\*\*, 223 \(1985\)](#).
- [12] W. H. Zurek, “Decoherence, einselection, and the quantum origins of the classical”, [Rev. Mod. Phys. \*\*75\*\*, 715 \(2003\)](#).
- [13] P. Stammer, J. Rivera-Dean, P. Tzallas, M. F. Ciappina, and M. Lewenstein, “Colloquium: Quantum optics of intense light–matter interaction”, [arXiv:2510.19045](#).
- [14] M. F. Ciappina, M. Y. Ivanov, M. Lewenstein, J. Rivera-Dean, P. Stammer, and P. Tzallas, “Quantum Optics and Quantum Electrodynamics of Strong Field Processes”, [arXiv:2509.26602](#).
- [15] P. Stammer, J. Rivera-Dean, A. Maxwell, T. Lamprou, A. Ordóñez, M. F. Ciappina, P. Tzallas, and M. Lewenstein, “Quantum Electrodynamics of Intense Laser-Matter Interactions: A Tool for Quantum State Engineering”, [PRX Quantum \*\*4\*\*, 010201 \(2023\)](#).
- [16] U. Bhattacharya, T. Lamprou, A. S. Maxwell, A. Ordóñez, E. Pisanty, J. Rivera-Dean, P. Stammer, M. F. Ciappina, M. Lewenstein, and P. Tzallas, “Strong–laser–field physics, non–classical light states and quantum information science”, [Reports Prog. Phys. \*\*86\*\*, 094401 \(2023\)](#).
- [17] M. Lewenstein, N. Baldelli, U. Bhattacharya, J. Biegert, M. F. Ciappina, T. Grass, P. T. Grochowski, A. S. Johnson, T. Lamprou, A. S. Maxwell, A. Ordóñez, E. Pisanty, J. Rivera-Dean, P. Stammer, and P. Tzallas, in [Springer Proc. Phys.](#) (2024), pp. 27–44.
- [18] L. Cruz-Rodriguez, D. Dey, A. Freibert, and P. Stammer, “Quantum phenomena in attosecond science”, [Nat. Rev. Phys. \*\*6\*\*, 691 \(2024\)](#).
- [19] M. Lewenstein, M. F. Ciappina, E. Pisanty, J. Rivera-Dean, P. Stammer, T. Lamprou, and P. Tzallas, “Generation of optical Schrödinger cat states in intense laser–matter interactions”, [Nat. Phys. \*\*17\*\*, 1104 \(2021\)](#).
- [20] J. Rivera-Dean, T. Lamprou, E. Pisanty, P. Stammer, A. F. Ordóñez, A. S. Maxwell, M. F. Ciappina, M. Lewenstein, and P. Tzallas, “Strong laser fields and their power to generate controllable high-photon-number coherent-state superpositions”, [Phys. Rev. A \*\*105\*\*, 033714 \(2022\)](#).
- [21] P. Stammer, “Theory of entanglement and measurement in high-order harmonic generation”, [Phys. Rev. A \*\*106\*\*, L050402 \(2022\)](#).

- [22] P. Stammer, J. Rivera-Dean, T. Lamprou, E. Pisanty, M. F. Ciappina, P. Tzallas, and M. Lewenstein, “High Photon Number Entangled States and Coherent State Superposition from the Extreme Ultraviolet to the Far Infrared”, *Phys. Rev. Lett.* **128**, 123603 (2022).
- [23] J. Rivera-Dean, T. Lamprou, E. Pisanty, M. F. Ciappina, P. Tzallas, M. Lewenstein, and P. Stammer, “Quantum state engineering of light using intensity measurements and postselection”, *Phys. Rev. A* **112**, 013110 (2025).
- [24] T. Sh. Iskhakov, A. M. Pérez, K. Yu. Spasibko, M. V. Chekhova, and G. Leuchs, “Superbunched bright squeezed vacuum state”, *Opt. Lett.* **37**, 1919 (2012).
- [25] M. Chekhova, G. Leuchs, and M. Żukowski, “Bright squeezed vacuum: Entanglement of macroscopic light beams”, *Opt. Commun.* **337**, 27 (2015).
- [26] P. R. Sharapova, G. Frascella, M. Riabinin, A. M. Pérez, O. V. Tikhonova, S. Lemieux, R. W. Boyd, G. Leuchs, and M. V. Chekhova, “Properties of bright squeezed vacuum at increasing brightness”, *Phys. Rev. Res.* **2**, 013371 (2020).
- [27] K. Y. Spasibko, D. A. Kopylov, V. L. Krutyanskiy, T. V. Murzina, G. Leuchs, and M. V. Chekhova, “Multiphoton Effects Enhanced due to Ultrafast Photon-Number Fluctuations”, *Phys. Rev. Lett.* **119**, 223603 (2017).
- [28] A. Gorlach, M. E. Tzur, M. Birk, M. Krüger, N. Rivera, O. Cohen, and I. Kaminer, “High-harmonic generation driven by quantum light”, *Nat. Phys.* **19**, 1689 (2023).
- [29] A. Rasputnyi, Z. Chen, M. Birk, O. Cohen, I. Kaminer, M. Krüger, D. Seletskiy, M. Chekhova, and F. Tani, “High-harmonic generation by a bright squeezed vacuum”, *Nat. Phys.* **20**, 1960 (2024).
- [30] S. Wang, S. Yu, X. Lai, and X. Liu, “High harmonic generation from an atom in a squeezed-vacuum environment”, *Phys. Rev. Res.* **6**, 033010 (2024).
- [31] M. E. Tzur, M. Birk, A. Gorlach, I. Kaminer, M. Krüger, and O. Cohen, “Generation of squeezed high-order harmonics”, *Phys. Rev. Res.* **6**, 033079 (2024).
- [32] S. Lemieux, S. A. Jalil, D. N. Purschke, N. Boroumand, T. J. Hammond, D. Villeneuve, A. Naumov, T. Brabec, and G. Vampa, “Photon bunching in high-harmonic emission controlled by quantum light”, *Nat. Photonics* **19**, 767 (2025).
- [33] J. Rivera-Dean, P. Stammer, M. F. Ciappina, and M. Lewenstein, “Structured Squeezed Light Allows for High-Harmonic Generation in Classical Forbidden Geometries”, *Phys. Rev. Lett.* **135**, 013801 (2025).
- [34] R. V. Gothelf, C. S. Lange, and L. B. Madsen, “High-order harmonic generation in a crystal driven by quantum light”, *Phys. Rev. A* **111**, 063105 (2025).
- [35] M. Even Tzur, M. Birk, A. Gorlach, M. Krüger, I. Kaminer, and O. Cohen, “Photon-statistics force in ultrafast electron dynamics”, *Nat. Photonics* **17**, 501 (2023).
- [36] M. Even Tzur and O. Cohen, “Motion of charged particles in bright squeezed vacuum”, *Light Sci. Appl.* **13**, 41 (2024).
- [37] J. Heimerl, A. Mikhaylov, S. Meier, H. Höllerer, I. Kaminer, M. Chekhova, and P. Hommelhoff, “Multiphoton electron emission with non-classical light”, *Nat. Phys.* **20**, 945 (2024).
- [38] J. Heimerl, A. Rasputnyi, J. Pölloth, S. Meier, M. Chekhova, and P. Hommelhoff, “Quantum light drives electrons strongly at metal needle tips”, *Nat. Phys.* **21**, 1899 (2025).
- [39] T. Lamprou, J. Rivera-Dean, P. Stammer, M. Lewenstein, and P. Tzallas, “Nonlinear Optics Using Intense Optical Coherent State Superpositions”, *Phys. Rev. Lett.* **134**, 013601 (2025).

- [40] S. Imai, A. Ono, and N. Tsuji, “Electron dynamics induced by quantum cat-state light”, [arXiv:2501.16801](#).
- [41] S. Imai, “Macroscopic Schrödinger-cat states of nonequilibrium electrons induced by cat-state optical driving and projective measurements on the light field”, [Phys. Rev. A \*\*113\*\*, 023702 \(2026\)](#).
- [42] J. Janszky and A. V. Vinogradov, “Squeezing via one-dimensional distribution of coherent states”, [Phys. Rev. Lett. \*\*64\*\*, 2771 \(1990\)](#).
- [43] M. Tavis and F. W. Cummings, “Exact Solution for an N-Molecule–Radiation-Field Hamiltonian”, [Phys. Rev. \*\*170\*\*, 379 \(1968\)](#).
- [44] I. I. Rabi, “Space Quantization in a Gyating Magnetic Field”, [Phys. Rev. \*\*51\*\*, 652 \(1937\)](#).
- [45] R. H. Dicke, “Coherence in Spontaneous Radiation Processes”, [Phys. Rev. \*\*93\*\*, 99 \(1954\)](#).
- [46] C. Genes, P. R. Berman, and A. G. Rojo, “Spin squeezing via atom-cavity field coupling”, [Phys. Rev. A \*\*68\*\*, 043809 \(2003\)](#).
- [47] A. E. B. Nielsen, U. V. Poulsen, A. Negretti, and K. Mølmer, “Atomic quantum superposition state generation via optical probing”, [Phys. Rev. A \*\*79\*\*, 023841 \(2009\)](#).
- [48] A. Kuzmich, K. Mølmer, and E. S. Polzik, “Spin Squeezing in an Ensemble of Atoms Illuminated with Squeezed Light”, [Phys. Rev. Lett. \*\*79\*\*, 4782 \(1997\)](#).
- [49] J. Hald, J. L. Sørensen, C. Schori, and E. S. Polzik, “Spin Squeezed Atoms: A Macroscopic Entangled Ensemble Created by Light”, [Phys. Rev. Lett. \*\*83\*\*, 1319 \(1999\)](#).
- [50] G. S. Agarwal and R. R. Puri, “Cooperative behavior of atoms irradiated by broadband squeezed light”, [Phys. Rev. A \*\*41\*\*, 3782 \(1990\)](#).
- [51] J. Gough and D. Rees, “Quantum Filtering for Squeezed Noise Inputs”, [arXiv:2601.12564](#).
- [52] K. Lemr and J. Fiurášek, “Conditional preparation of arbitrary superpositions of atomic Dicke states”, [Phys. Rev. A \*\*79\*\*, 043808 \(2009\)](#).
- [53] J. K. Stockton, R. van Handel, and H. Mabuchi, “Deterministic Dicke-state preparation with continuous measurement and control”, [Phys. Rev. A \*\*70\*\*, 022106 \(2004\)](#).
- [54] C. Genes and P. R. Berman, “Generating conditional atomic entanglement by measuring photon number in a single output channel”, [Phys. Rev. A \*\*73\*\*, 013801 \(2006\)](#).
- [55] Y.-l. Zhang, C.-s. Yang, C.-l. Zou, T. Xia, G.-C. Guo, and X.-B. Zou, “Quantum state preparation of an atomic ensemble via cavity-assisted homodyne measurement”, [J. Phys. B At. Mol. Opt. Phys. \*\*52\*\*, 215003 \(2019\)](#).
- [56] S. Massar and E. S. Polzik, “Generating a Superposition of Spin States in an Atomic Ensemble”, [Phys. Rev. Lett. \*\*91\*\*, 060401 \(2003\)](#).
- [57] R. McConnell, H. Zhang, S. Čuk, J. Hu, M. H. Schleier-Smith, and V. Vuletić, “Generating entangled spin states for quantum metrology by single-photon detection”, [Phys. Rev. A \*\*88\*\*, 063802 \(2013\)](#).
- [58] R. McConnell, H. Zhang, J. Hu, S. Čuk, and V. Vuletić, “Entanglement with negative Wigner function of almost 3,000 atoms heralded by one photon”, [Nature \*\*519\*\*, 439 \(2015\)](#).
- [59] W. Chen, J. Hu, Y. Duan, B. Braverman, H. Zhang, and V. Vuletić, “Carving Complex Many-Atom Entangled States by Single-Photon Detection”, [Phys. Rev. Lett. \*\*115\*\*, 250502 \(2015\)](#).
- [60] T. Vanderbruggen, S. Bernon, A. Bertoldi, A. Landragin, and P. Bouyer, “Spin-squeezing and Dicke-state preparation by heterodyne measurement”, [Phys. Rev. A \*\*83\*\*, 013821 \(2011\)](#).

- [61] T. Vanderbruggen, R. Kohlhaas, A. Bertoldi, E. Cantin, A. Landragin, and P. Bouyer, “Feedback control of coherent spin states using weak nondestructive measurements”, *Phys. Rev. A* **89**, 063619 (2014).
- [62] G. Tóth and M. W. Mitchell, “Generation of macroscopic singlet states in atomic ensembles”, *New J. Phys.* **12**, 053007 (2010).
- [63] N. Behbood, F. Martin Ciurana, G. Colangelo, M. Napolitano, G. Tóth, R. J. Sewell, and M. W. Mitchell, “Generation of macroscopic singlet states in a cold atomic ensemble”, *Phys. Rev. Lett.* **113**, 093601 (2014).
- [64] I. Bouchoule and K. Mølmer, “Preparation of spin-squeezed atomic states by optical-phase-shift measurement”, *Phys. Rev. A* **66**, 043811 (2002).
- [65] I. D. Leroux, M. H. Schleier-Smith, H. Zhang, and V. Vuletić, “Unitary cavity spin squeezing by quantum erasure”, *Phys. Rev. A* **85**, 013803 (2012).
- [66] S. J. Masson and S. Parkins, “Rapid Production of Many-Body Entanglement in Spin-1 Atoms via Cavity Output Photon Counting”, *Phys. Rev. Lett.* **122**, 103601 (2019).
- [67] R. V. Gothelf, L. B. Madsen, and C. S. Lange, “Limitations of an approximative phase-space description in strong-field quantum optics”, [arXiv:2602.04370](https://arxiv.org/abs/2602.04370).
- [68] K. Kraus, *States, Effects, and Operations: Fundamental Notions of Quantum Theory*, edited by A. Böhm, J. D. Dollard, and W. H. Wootters, Vol. 190, Lecture Notes in Physics (Springer Berlin Heidelberg, Berlin, Heidelberg, 1983).
- [69] H. M. Wiseman and G. J. Milburn, *Quantum Measurement and Control* (Cambridge University Press, Cambridge, Nov. 2009).
- [70] C. W. Helstrom, “Quantum detection and estimation theory”, *J. Stat. Phys.* **1**, 231 (1969).
- [71] A. Holevo, *Probabilistic and Statistical Aspects of Quantum Theory* (Edizioni della Normale, Pisa, 2011).
- [72] R. L. Stratonovich, “On Distributions in Representation Space”, *Zh. Eksp. Teor. Fiz.* **31**, 1012 (1956).
- [73] C. Brif and A. Mann, “Phase-space formulation of quantum mechanics and quantum-state reconstruction for physical systems with Lie-group symmetries”, *Phys. Rev. A* **59**, 971 (1999).
- [74] G. Tóth, “Multipartite entanglement and high-precision metrology”, *Phys. Rev. A* **85**, 022322 (2012).
- [75] P. Hyllus, W. Laskowski, R. Krischek, C. Schwemmer, W. Wieczorek, H. Weinfurter, L. Pezzè, and A. Smerzi, “Fisher information and multiparticle entanglement”, *Phys. Rev. A* **85**, 022321 (2012).
- [76] M. Gessner, A. Smerzi, and L. Pezzè, “Metrological Nonlinear Squeezing Parameter”, *Phys. Rev. Lett.* **122**, 090503 (2019).
- [77] Z. Ren, W. Li, A. Smerzi, and M. Gessner, “Metrological Detection of Multipartite Entanglement from Young Diagrams”, *Phys. Rev. Lett.* **126**, 80502 (2021).
- [78] J. Davis, M. Kumari, R. B. Mann, and S. Ghose, “Wigner negativity in spin-j systems”, *Phys. Rev. Res.* **3**, 033134 (2021).
- [79] M. Kitagawa and M. Ueda, “Squeezed spin states”, *Phys. Rev. A* **47**, 5138 (1993).
- [80] C. Groiseau, S. J. Masson, and S. Parkins, “Generation of spin cat states in an engineered Dicke model”, *Phys. Rev. A* **104**, 053721 (2021).
- [81] C. Groiseau, “Generation of Large Kitten states via thermally driven dissipative freezing”, [arXiv:2509.00601](https://arxiv.org/abs/2509.00601).

- [82] D. M. Greenberger, M. A. Horne, and A. Zeilinger, in *Bell's Theorem, Quantum Theory and Conceptions of the Universe*, 3 (Springer Netherlands, Dordrecht, 1989), pp. 69–72.
- [83] W. Magnus, “On the exponential solution of differential equations for a linear operator”, *Commun. Pure Appl. Math.* **7**, 649 (1954).
- [84] J. H. Shirley, “Solution of the Schrödinger Equation with a Hamiltonian Periodic in Time”, *Phys. Rev.* **138**, B979 (1965).
- [85] H. Sambe, “Steady States and Quasienergies of a Quantum-Mechanical System in an Oscillating Field”, *Phys. Rev. A* **7**, 2203 (1973).
- [86] S. Rahav, I. Gilyad, and S. Fishman, “Effective Hamiltonians for periodically driven systems”, *Phys. Rev. A* **68**, 013820 (2003).
- [87] A. Eckardt and E. Anisimovas, “High-frequency approximation for periodically driven quantum systems from a Floquet-space perspective”, *New J. Phys.* **17**, 093039 (2015).
- [88] P. Forn-Díaz, L. Lamata, E. Rico, J. Kono, and E. Solano, “Ultrastrong coupling regimes of light-matter interaction”, *Rev. Mod. Phys.* **91**, 025005 (2019).
- [89] H. Vahlbruch, M. Mehmet, K. Danzmann, and R. Schnabel, “Detection of 15 dB Squeezed States of Light and their Application for the Absolute Calibration of Photoelectric Quantum Efficiency”, *Phys. Rev. Lett.* **117**, 110801 (2016).
- [90] C. W. Gardiner and M. J. Collett, “Input and output in damped quantum systems: Quantum stochastic differential equations and the master equation”, *Phys. Rev. A* **31**, 3761 (1985).
- [91] A. H. Kübler and K. Mølmer, “Input-Output Theory with Quantum Pulses”, *Phys. Rev. Lett.* **123**, 123604 (2019).
- [92] A. I. Lvovsky and M. G. Raymer, “Continuous-variable optical quantum-state tomography”, *Rev. Mod. Phys.* **81**, 299 (2009).
- [93] T. Tyc and B. C. Sanders, “Operational formulation of homodyne detection”, *J. Phys. A: Math. Gen.* **37**, 7341 (2004).
- [94] M. G. Raymer, J. Cooper, H. J. Carmichael, M. Beck, and D. T. Smithey, “Ultrafast measurement of optical-field statistics by dc-balanced homodyne detection”, *J. Opt. Soc. Am. B* **12**, 1801 (1995).